Chapter 8

Surface Modification of Magnesium and its Alloys Using Anodization for Orthopedic Implant Application

Hamouda M. Mousa, Chan Hee Park and Cheol Sang Kim

Additional information is available at the end of the chapter

http://dx.doi.org/10.5772/66341

Abstract

Magnesium (Mg) as a biodegradable implant brings a revolution in medical field application, especially in bone implant and stent application. Biodegradability of Mg has attracted attentions of researchers to avoid secondary surgery to remove the implant materials after healing process. Various advantages of Mg make it suitable for medical application such as density, good mechanical properties and biodegradation. However, Mg biodegradability must be controlled to meet tissue-healing period of time because of the high degradation in a physiological environment. Fast corrosion and high alkalinity due to hydrogen release induce tissue inflammation, which limits its clinical applications. Many techniques are applied to the Mg surface to improve surface biocompatibility and control its biodegradability. This chapter focuses on anodization of Mg and its alloys to improve corrosion resistance and biocompatibility for orthopedic application. Mg coating with thin film apatite could enhance the biocompatibility and increase osseointegration formation in the bone fracture side. Evaluation of the required anodized film discussed in the chapter such as chemical composition, biodegradability and biocompatibility.

Keywords: magnesium, anodization, SBF, b106048iocompatibility, biodegradable metals

1. Introduction

Biodegradable metallic implant material has received considerable attention in biomedical field such as blood vessels or orthopedic application as load-bearing implant [1, 2]. Mg is suitable for implant application in human body, for example, Mg stent, bone fixation screw, microclips in laryngeal microsurgery, bone fixation and wound-closing devices, as shown in **Figure 1**. Mg has many appealing properties such as light weight, high strength-to-weight ratio, good castability and osteoconductivity [3]. However, Mg has limitations mainly due to

its high surface chemical reactivity resulting in high degradation rate [4]. The poor corrosion resistance of Mg limits its clinical applications, as hydrogen evaluation is one of the corrosion products that increase alkalinity of the surrounded media and causing inflammation of the surrounding tissues due to the formation of gas pockets [5, 6]. The high degradation rate may eventually hinder the bone formation and hamper the long-term success of the implants and decrease its bioactivity as well as loss its mechanical properties [7]. Mg-based implants exhibited rough surfaces as well as shallow pits and small cavities after one day of implantation, which formed during the on-going corrosion process to form cracks until the implant totally dissolves [8]. The high purity of Mg finds to corrode uniformly *in vivo* [9]. Biodegradable metals (BMs) are typically degraded through the corrosion process when exposed to a corrosive media. For example, when BMs especially Mg implanted in human body, the corrosion/degradation process generated electrochemically in different reactions of metals with an electrolyte and produced metal oxides and hydroxides [7]. Moreover, hydrogen gas evaluation is a combined corrosion product; these reactions could be represented in the following chemical equations at anodic dissolution of Mg and the cathodic reaction [10].

$$Mg \rightarrow Mg^{2+} + 2e^{-} \quad \text{(anodic reaction)} \tag{1}$$

$$2H_2O + 2ne^{-} \rightarrow H_2 + 2OH \quad \text{(cathodic reaction)} \tag{2}$$

$$2H_2O + O_2 + 4e^{-} \rightarrow 4OH^{-} \quad \text{(cathodic reaction)} \tag{3}$$

$$Mg + 2H_2O \rightarrow Mg(OH)_2 + H_2 \quad \text{(overall reaction)} \tag{4}$$

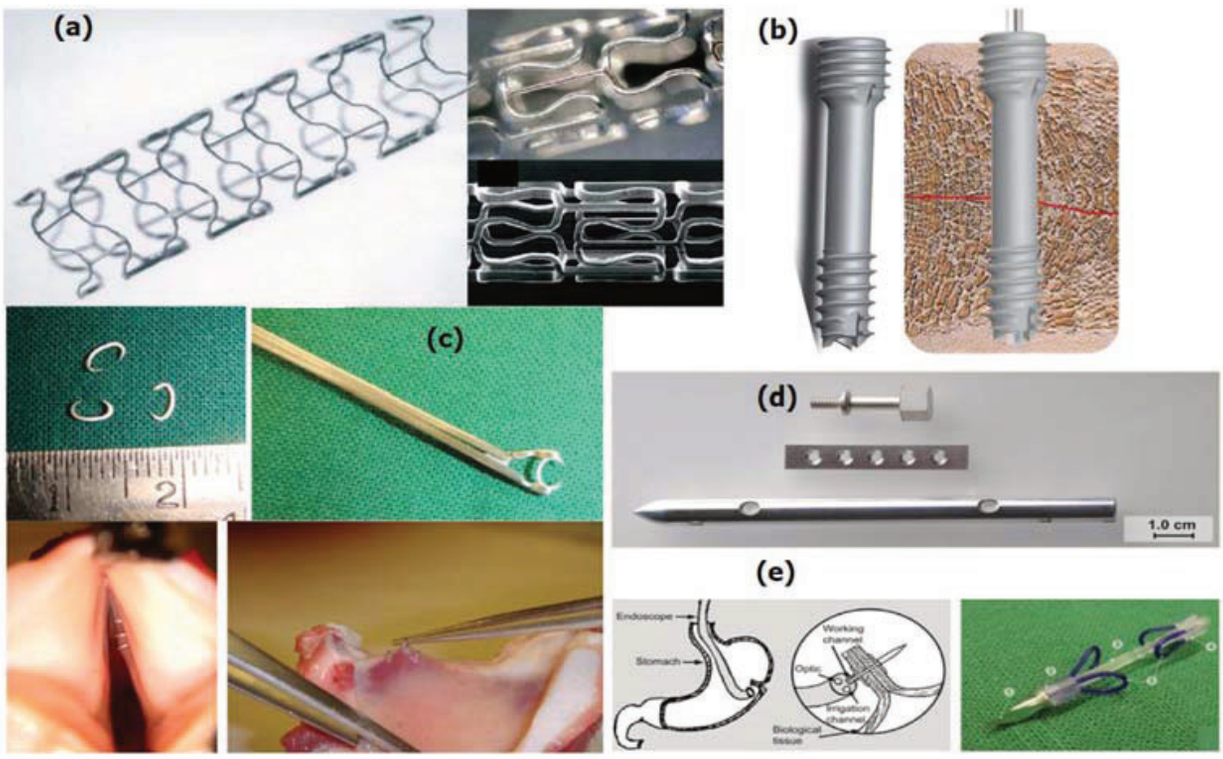

Figure 1. Different applications of Mg-based implant material: (a) cardiovascular Mg stents, (b) MAGNEZIX screw, (c) microclip for laryngeal microsurgery (pure magnesium), (d) biodegradable orthopedic implants and (e) wound-closing devices (WZ21) [11].

http://dx.doi.org/10.5772/66341

Surface modification is considered one of the most useful and effective methods to control the initial degradation of Mg and its alloys [12]. **Table 1** summarizes the previous research on Mg coating with different applied techniques and chemical composition. Among these techniques, anodization is a widely and traditional process for metal surface modification to improve the physiochemical properties of metals [13]. A suitable electrolyte of anodization for the specific application of Mg is one of the essential requirements when it employed. For example, hydroxyapatite (HA) is a bioactive ceramic material which widely used in bone application [14]. HA could be engineered to mimic the three-dimensional inorganic component of the bone which is composed of 65% of bone. The structure of HA could provide the space and area necessary for vascularization and tissue regeneration. In this chapter, HA coating with different nanostructures (nanoplates/nanospheres) by means of anodization is discussed with the associated mechanical integrity, biodegradability and biocompatibility. Formation of nanoplates could promote the osseointegration and eliminate the mismatching of the implant material. Accordingly, using stimulated body fluid (SBF) finds to form apatite film on the surface of Mg in a short duration.

Substrate	Experimental and coating type	Reference
Mg-Zn-Ca alloy	Fabrication of hydroxyapatite nanorod on MAO coating to increase bioactivity and improve the biodegradation behavior	[15]
Mg-1.0Ca alloys	Sodium phytate ($Na_{12}Phy$) used as an electrolyte with anodic coatings fabricated in an organic phosphate containing solution on the Mg-1.0Ca alloys. In order to achieve a proper degradation rate, acceptable biocompatibility and good antibacterial ability	[16]
AZ31B	Different electrolytes such as KOH, Na_2SiO_3 and $Na_2B_4O_7$ were used for pulsed DC micro-arc oxidation (MAO) process	[17]
Mg-Zn-Ca	A porous bioceramic containing tricalcium phosphate in (TCP) coating was prepared by (MAO) at different voltages	[18]
Pure Mg	Anodic oxide coatings were prepared using 0.3 M NaOH + 15 g/l ZrO_2 and 3 M NaOH + 15 g/l ZrO_2	[19]
AZ31B	A chemical conversion film on magnesium alloys is proposed based on the interaction of a deep eutectic solvent (DES) with the substrate	[20]
Mg-3Zn	A nanostructured hydroxyapatite (HA) coating was grown on through the electrophoretic deposition (EPD) technique	[21]
ZK61	MAO coating film with low crystallinity is composed of MgO, Mg_2SiO_4 and $Mg_2Si_2O_6$ employed	[22]
AZ31	A dopamine-induced hydroxyapatite coating was successfully developed on the AZ31 alloy	[23]
AZ31	Use of a microwave-assisted coating technology to improve the *in vitro* corrosion resistance and biocompatibility of AZ31Mg alloy	[24]
Pure Mg	A simple strontium phosphate (SrP) conversion coating process was developed to protect magnesium (Mg) from the initial degradation postimplantation	[25]
AZ31	A Si-doped calcium phosphate coating was achieved via pulse ED on the AZ31 alloy. A novel dual-layer structure was observed with a porous lamellar-like and outer block-like apatite layer	[26]

Table 1. Summary of Mg surface modification techniques.

2. Anodization process

Anodization is an electrochemical process that converts the metal surface into a decorative, durable, corrosion-resistant and anodic oxide finish [27]. The coating thicknesses can range from 5 to 200 μm. Typically, anodic oxide layers grow depending on the process time and applied voltages [28], leading to a direct dependence of the oxide thickness on the applied voltage as shown in **Figure 2**. For metals and alloys with barrier-type anodic oxide films, blocking electron conduction under anodic polarization an anodization can be carried out at high voltages in aqueous solution [29]. Therefore, thick oxides that can be grown on the conductive oxide layers on the metal surface by means of anodization are limited to the applied voltage. The applied voltage is lower than that at which water can dissociated with evaluation of oxygen, whereas, above that potential water tends to decompose rather than thickening of the oxide layer. For example, Mg has potential and conductivity; therefore, the resulting potential while anodization applied depends mainly on the electrolyte composition [29]. The incorporation of electrolyte materials with growing oxide/hydroxide layers can form an oxide layers that have higher blocking efficiency

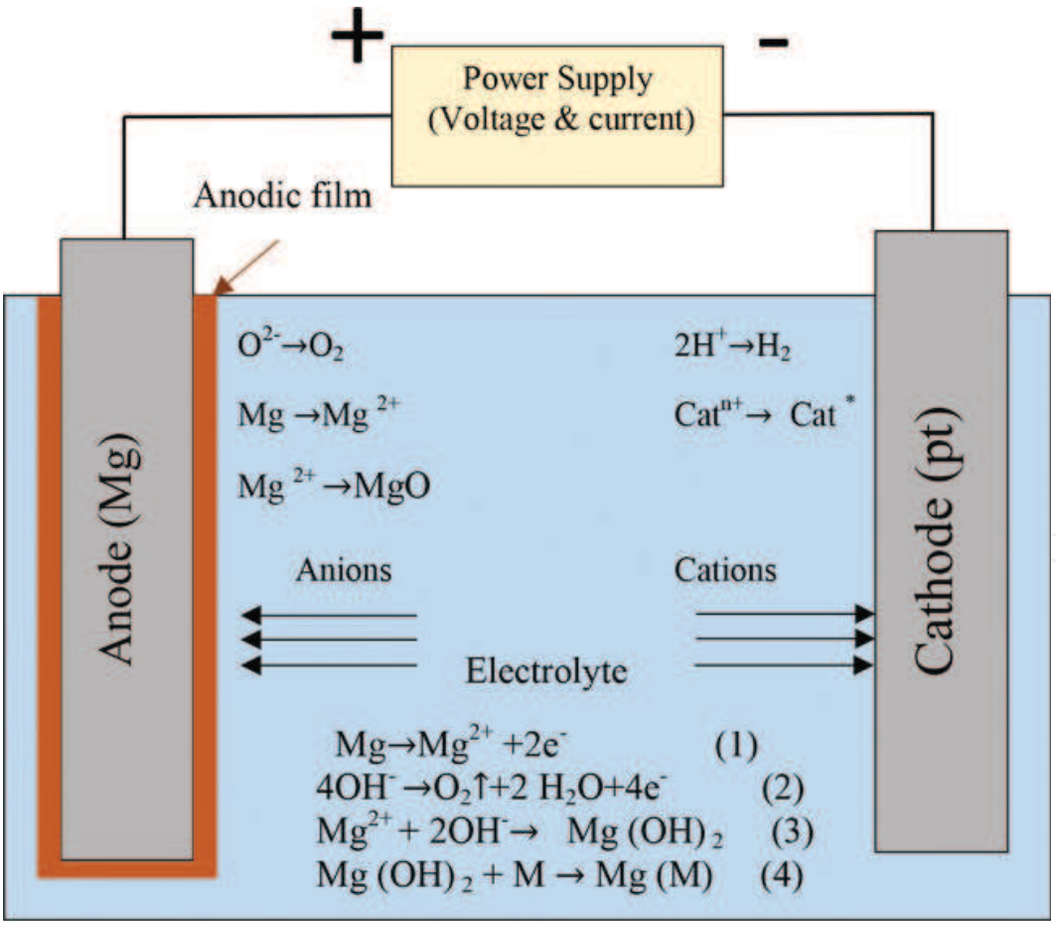

Figure 2. Illustrative diagram shows the mechanism of anodization technique. Mg acts as an anode where it converted to Mg^{2+} then reacts with O^{2-} to form MgO in the presence of OH ions, $Mg(OH)_2$ formation on the metal surface and hydrogen formed the surrounding cathode part.

http://dx.doi.org/10.5772/66341

toward the corrosive ions. Therefore, thick and compact film is a challenge for Mg interface anodization treatment, however, obtaining a low Pilling-Bedworth ratio for the formed anodized film [30]. This could cause an internal stresses on the generated anodic film and subsequently crack defects [31]. The degree of porosity and oxide layer quality could be enhanced by anodization parameter adjustment. These parameters include electrolyte composition, anodization voltage, current and time [32]. Anodization performed in different baths, for example an alkaline electrolyte is based on potassium hydroxide, phosphate, fluoride, or silicate-containing baths. Electrolyte composition plays a critical role not only to enable anodization at high voltage but also to reduce Mg dissolution during the process [33]. There are various methods and techniques with a wide range of patents to produce such anodic films [34]. In addition to anodization approaches which are mainly used to thicken the native oxide/hydroxide films on metal surfaces, dedicated anodization approaches have been explored to obtain nanoporous oxide layers. Therefore, the appropriate electrolyte composition leads to competition between Mg dissolution during anodization and anodic oxide film growth. Thus, optimized parameters based on the electrochemical process self-organized growth of nanoporous or nanotubular oxide layers could performed; however, it is still at early stage for Mg and its alloys [35, 36]. **Table 2** summarizes different Mg alloy anodization/PEO on different electrolytes with the resulted film thickness and chemical composition and the mainly electrochemical corrosion parameters (E_{corr} and i_{corr}).

Substrate	Electrolyte	Thickness	Layer composition	i_{corr}	E_{corr}	Refs.
AZ91D	PEO in NaOH + $(NaPO_3)_6$ + $Ca(H_2PO_2)_2$ solution	3–5 μm	Mg, Al, P and Ca and little crystallized MgO	X	X	[40]
AZ91D	PEO in Na_2SiO_3 + $(NaPO_3)_6$ + $Ca(H_2PO_2)_2$ solution	8–10 μm	Mg, Al, Si, P and Ca, crystallized Mg_2SiO_4 and MgO	X	X	[2]
AM50	PEO in $CaOH_2$ + Na_3PO_4 solution in different mass ratios	in the range of 20–70 μm	MgO, $Mg_3(PO4)_2$, amorphous Ca-phases, $CaH(PO_4)_2$, CaO_2	X	X	[41]
AZ91	NaOH	1–2 μm	MgO and Mg	X	X	[42]
ZK60	100 g/l NaOH + 20 g/l $Na_2B_4O_7{\cdot}10H_2O$ + 50 g/l $C_6H_5Na_3O_7{\cdot}2H_2O$ + 60 g/l $Na_2SiO_3{\cdot}9H_2O$	10–60 μm	MgO and Mg_2SiO_4	1.829×10^{-2} (mA/cm^2)	−1.46	[43]
AZ31	SBF solution	5–25 μm	MgO, Mg and amorphous apatite	103 to 0.9 μA/cm^2	−1.39 to −1.45	[44]
AZ31	(ZrO_2-NPs) dispersed in SBF	X	Mg, MgO, ZrO_2, and $Mg_2Zr_5O_{12}$	−1.46 to −1.38	2.796 to 1.9	[45]
AZ31	(SBF solution + HA) then hydrothermal in 5 M NaOH at 60°C for 2 h	X	Mg, MgO, CaO and HA	7.6 to 1025 nA/cm^2	1.52 to 1.31	[46]

Table 2. Anodization of Mg alloys in different electrolyte.

3. Surface morphology and composition

The design of surface morphology structure of biodegradable implant is an important factor since the interconnection of biomaterial interface with surrounding tissues is important for implant engagement and cell attachment [37]. In bone implant, nanoplate and nanosphere structure of HA coating as a biomimetic films are considered for the Mg coating interface, which is characterized by mimicking that of bone [38]. **Figure 3a** shows the nanoplates formation on the surface of AZ31 Mg alloy by the anodization method in SBF solution at 50 V and 30 mA with a process time of 10 min followed by the hydrothermal process in NaOH solution at 60°C for 2 h. However, adding HA powder to SBF solution resulted in nanosphere structure. Natural bone consists of HA nanocrystals in a plate-like shape with a length of 30–200 nm and a thickness of 2–7 nm [39]. As a result, designing HA films with the specific orientation and morphology is an important approach to improve Mg biological properties such as bioactivity and mimic that on natural bone. Furthermore, such nanoplates can promote the porosity of the implant interface, as a result avoid a mechanical mismatch between the hosts and implant interface, stress shield effect can be eliminated by altering surface porosity.

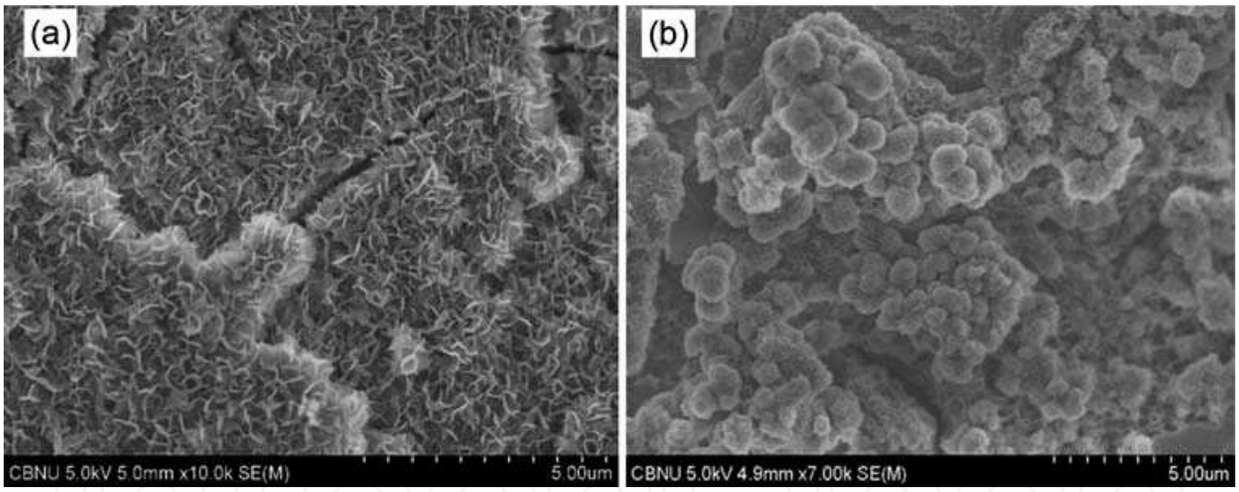

Figure 3. Surface morphology of anodized AZ31 Mg alloy in different electrolytes followed by the hydrothermal process in NaOH at 60°C for 2 h and SBF for 2 days at 37°C: (a) SBF as an electrolyte resulted in nanoplates morphology and (b) (SBF-10 g/l HA) resulted in nanospheres structure.

The chemical composition of HA coating finds is composed of Mg, MgO, HA and CaO peaks as shown in XRD peaks in **Figure 4a**. Furthermore, FT-IR spectra can indicate the outer HA film formation as shown in **Figure 4b**. The bands at a wave number of around 530 cm^{-1} is assigned to PO_4^{3-} in HA at the vibration of (ν_4) and at the vibration of (ν_3) around peaks of 1070 cm^{-1}. On the other hand, hydroxyl group absorption of HA is located at 3703 cm^{-1} [47], in addition to the

http://dx.doi.org/10.5772/66341

stretching ν(OH) that is observed at 3550, 3489 and 3412 cm^{-1}. The bands at 1147, 1070, 986 and 877 cm^{-1} are assigned to the P-O stretching vibration in the HPO_4^{2-} groups, respectively. The CO_3^{2-} group is located at 1386 cm^{-1} [26].

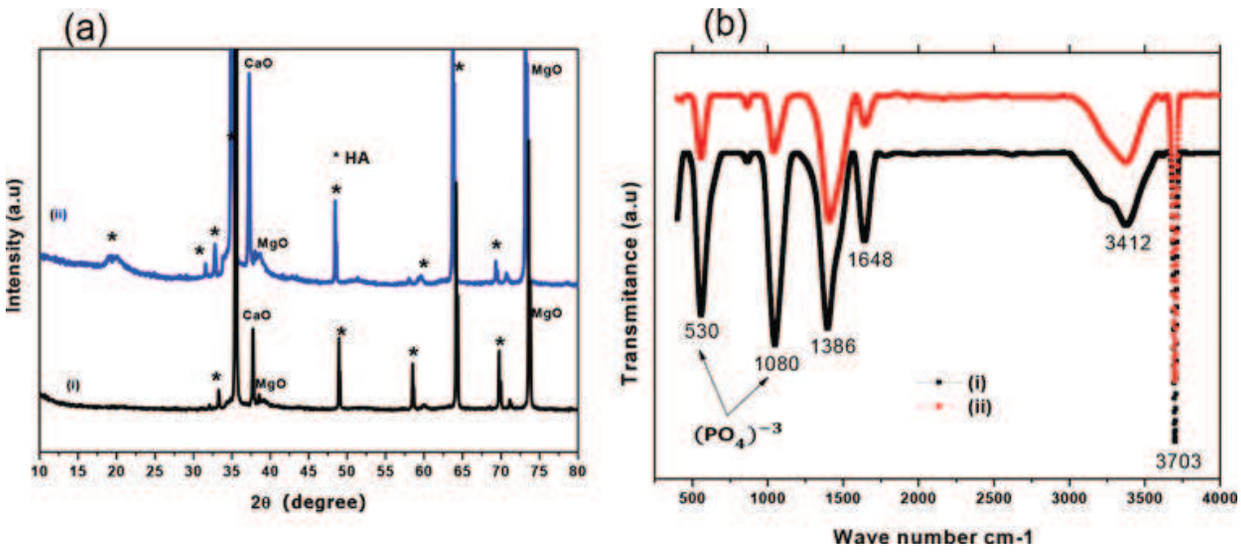

Figure 4. XRD patterns and FTIR spectra of the surface treatment samples, two anodized samples in (i) SBF solution and (ii) SBF/HA solution followed by the hydrothermal process according to reference [46].

4. Mechanical integrity

Mechanical tuning is one of the most effective factors for biodegradable Mg implant in load-bearing application and stent application [48]. Basically, implant materials act as a mechanical support during the healing process thereafter degrade and loss their mechanical properties. Because of that the chemical and mechanical stabilities of implant materials during the healing period are critically important. While implants are exposed to human body fluid, it often experiences considerable loadings and, thus, may undergo environmentally assisted cracking (stress corrosion cracking (SCC) and corrosion fatigue). **Figure 5** shows the mechanical behavior of Mg implant *in vivo* for 12 weeks of implantation and the resulted tensile strength. The coated samples with HA indicated a higher mechanical stability than uncoated samples. The degradation volumes of the bare and HA-coated Mg specimens after 6 and 12 weeks of implantation find that the coated samples have lower degradation with addition protection (**Figure 5b**). The concept of the mechanically tuned with degradation rate during tissue regeneration is illustrated in **Figure 5c**. In period of 1–7 days, inflammation process, hematoma formation with atypical inflammatory response, occurs. Next stage repairs, hematoma, granulation tissue, connective tissue, cartilage, mineralization, woven bone, continuous for 3–6 months depend on the fracture position and type. In the final stage, remodeling, woven bone is replaced by cortical bone and the medullary cavity is restored, which persists for several years.

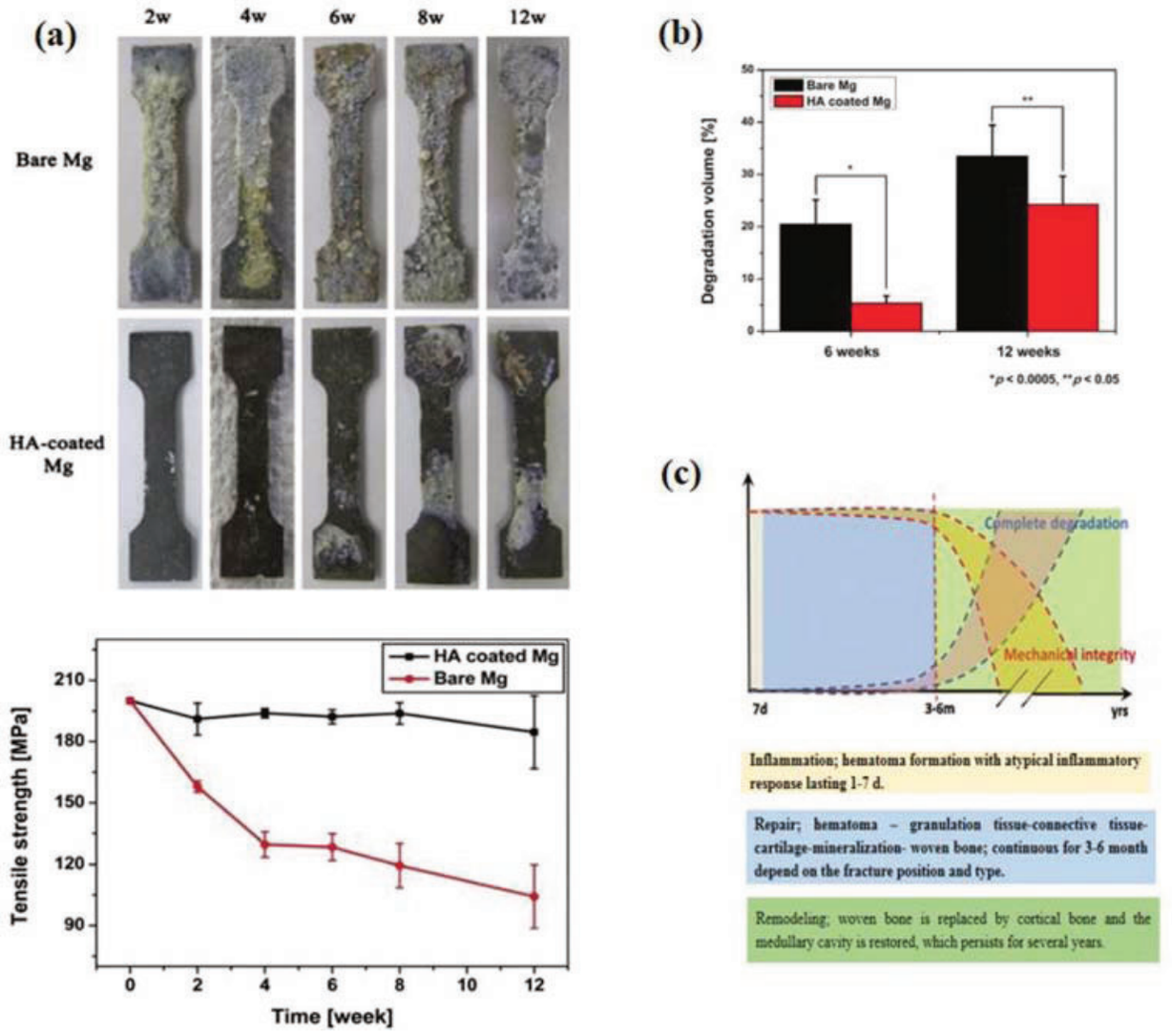

Figure 5. (a) *In vivo* evaluation of the mechanical and degradation properties of Mg coated with calcium orthophosphate coatings. (a) Optical images of the HA coated and bare samples at different implantation times at top and tensile strength of the HA-coated Mg samples comparing to the bare one after interval time. Reprinted from reference [49]. (b) Degradation volumes of the bare and HA-coated Mg specimens after 6 and 12 weeks of implantation [50]. (c) The schematic diagram of degradation behavior and the change of mechanical integrity of BM implants during the bone healing process [51].

5. Biodegradation evaluation

5.1. Electrochemical evaluation

Electrochemical polarization is an efficient technique used to evaluate metal corrosion potential in a short duration. Metals are commonly performed using electrochemical corrosion tests in SBF solution (pH = 7.4) at 37°C to mimic that of human blood plasma. The experimental setup consisted of three conventional electrodes within a cell, which named as working electrode, a saturated calomel electrode (SCE), or Ag/AgCl as a reference electrode, third is counter

electrode such as a platinum wire. The experiment is conducted and monitored the current density as a function of the free open-circuit potential using the potentiostat of an electrochemical device. Initially, the samples are exposed to the solution for 10–20 min, a scan rate (mV/s) of the potentiodynamic polarization test is main parameter when test was performed. Corrosion current density (i_{corr}) could be estimated from the linear fit and Tafel extrapolation to the cathodic and anodic parts of the polarization curves. Thereafter, the corrosion rate can be calculated based on Faraday's laws.

$$CR = 3.2710^{-3}\frac{Ewi_{corr}}{\rho} \tag{5}$$

where Ew is the equivalent weight of the corroding species in grams and ρ is the density of the corroding material in g/cm^3.

Faraday's laws assume a uniform corrosion in terms of the penetration, here the corrosion current (i_{corr}) is an effective factor in the corrosion rate and therefore the resulted value does not typically indicate an absolute corrosion rate for Mg. However, it represents indication of the corrosion distortion, which occurs at a selected point in time, in terms of current density. It is seldom in Mg and its alloys to degrade uniformly. The corrosion rate expressed with a current density value is highly accurate and can be considered to have the highest resolution of all methods. Current could be originating from a different local site on the surface and the method is considered as short-term and destructive one. In addition to the potentiodynamic polarization technique, it is essential to understand the mechanism of the corrosion rate; it may not suitable as a good indication for long-term corrosion rates. Electrochemical impedance spectroscopy (EIS) is a powerful tool that is used to evaluate a different application such as biosensors and conductivity as well as corrosion resistance of different metals using the frequency response of AC polarization [52]. EIS conducted with a range of low magnitude polarizing voltages that cycle from a peak anodic to peak cathodic voltage spanning a spectra of voltage frequencies. However, the technique has different components to understand the corrosion resistance of a metal surface. The components such as capacitance and resistance are obtained for each frequency and can then be used to explain a number of phenomena and properties of the metal surface. A determination of the corrosion rate is possible when the EIS determined polarization resistance (R_{polar}) parameter at the zero frequency limit is used. The R_{polar} is inversely proportional to the current density (j_{corr}) as described by the Stern-Geary relationship [44].

$$j_{corr} = \frac{\beta a \beta c}{2.303 R\text{polar}(\beta a + \beta c)} \tag{6}$$

where βa and βc are the anodic and cathodic Tafel slopes, respectively.

A corrosion rate can be determined by transferring the current using EIS, the primary function of performing EIS on Mg and its alloys in an electrolytic solution is the identification and quantification of the formation behavior of corrosion layers which produced by the corrosion process. However, EIS results have some limitations as it can be affected by the Mg dissolution at low frequencies and therefore the chosen equivalent circuit. As a result, to employ EIS

properly, a deep understanding of the corrosion processes takes place through the process and the best model. **Figure 6a** shows the potentiodynamic polarization curve of bare samples and anodized ones in SBF and SBF/ZrO_2 NPs as an electrolyte with the resulted potential and current density. Moreover, EIS results in terms of Nyquist plot and bode diagrams are shown in **Figure 6b** and **c**. Both techniques find corrosion resistance in anodized samples comparing to the bare samples.

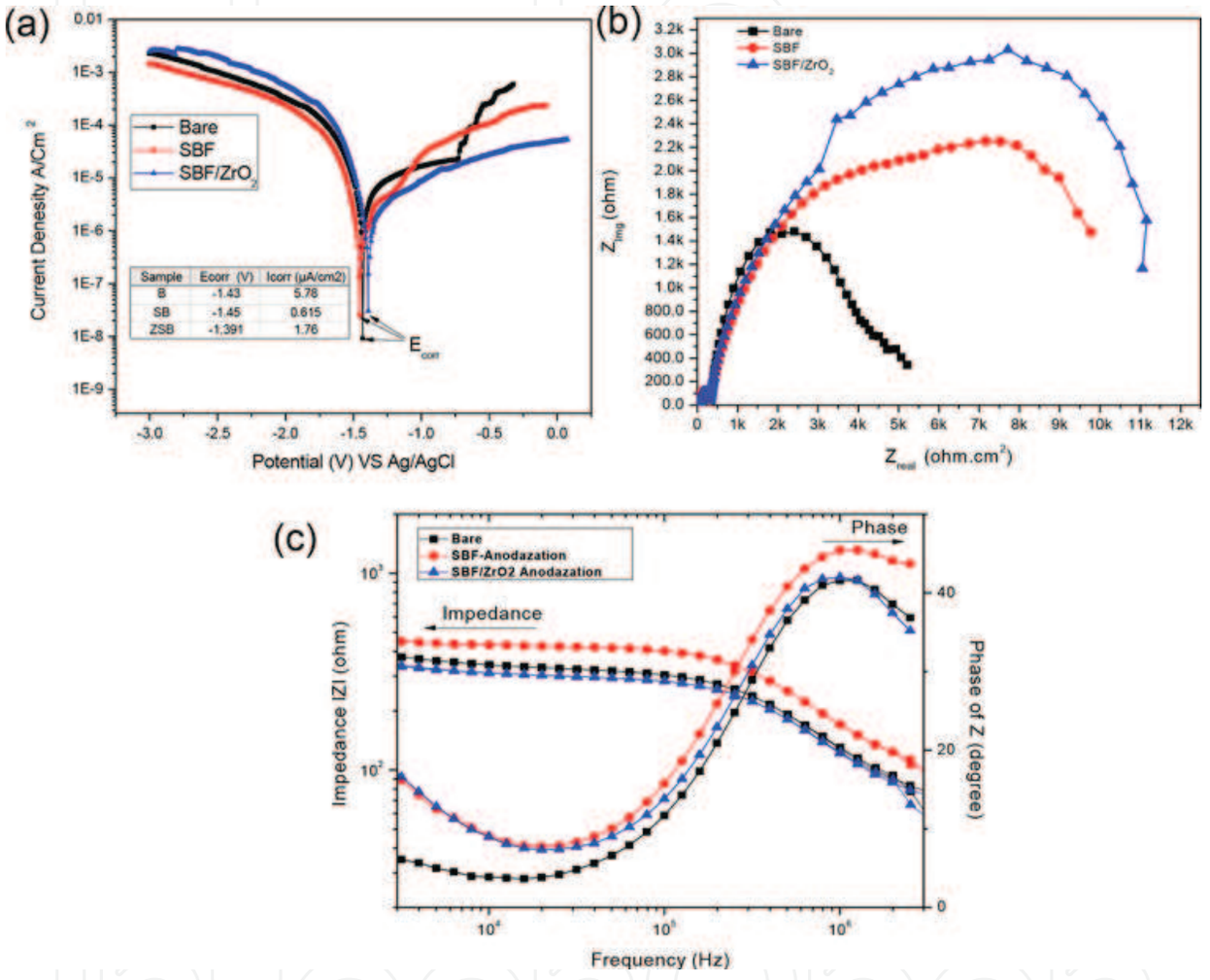

Figure 6. Corrosion evaluation of AZ31 Mg and anodizing samples in the SBF and SBF/ZrO_2 NP electrolyte. Test was performed in SBF solution at 37°C under a three-electrode system where Mg samples act as an electrode, platinum as a counter electrode and Ag/AgCl as a reference electrode. (a) Potentidynamic polarization curves, (b) Nyquist plot and (c) Bode plot diagrams.

5.2. *In vitro* immersion test

In this technique, an *in vitro* degradation rate in terms of mass loss is evaluated, before sample sterilization the initial weight of the samples was recorded. Then samples were immersed in a ratio of 30:1 volume to a weight ratio of SBF solution or Dulbecco's modified eagle's medium (DMEM) supplemented with 10% fetal bovine serum (FBS) for 168 h (1 week) under cell culture conditions (37°C, 20% O_2, 5% CO_2 and 95% humidity). The immersion medium recommended to be changed every 2–3 days to mimic the semistatic immersion test and to

http://dx.doi.org/10.5772/66341

avoid saturation effects according to the standard ASTM-G31-72. After immersion time, the formed corrosion products were removed by treating the corroded disc with chromic acid (200 g/L Cr_2O_3 + 10 g/L $AgNO_3$) at least for 20 min at room temperature [52].

Finally, the degradation rate (DR) was calculated in mm/year using the equation [53]:

$$\mathrm{DR} = 8.7610^4 \frac{\Delta g}{A.t.\rho} \tag{7}$$

where Δg is the change in weight by grams, A is the exposed surface area of the sample in cm^2, t is the immersion time in hours and ρ is the density in g/cm^3.

While exposure of the Mg substrate to aqueous solution generates H_2 and OH^- ions along the process of its degradation reaction with the medium, because of that the fluid pH value tends to be increase around the Mg surface. However, the instability of Mg occurs at pH values less than 11, a soluble compound formation with most inorganic ions would inhibits the formation of passive films of magnesium hydroxide in the biological environment. Moreover, the released Mg ions are another factor to indicate the dissolution of Mg in the aqueous solution process according to Eq. (8).

$$\mathrm{Mg} + 2\mathrm{H_2O} \rightarrow \mathrm{Mg^{+2}} + 2\mathrm{OH} + \mathrm{H_2}\uparrow \tag{8}$$

There are various corrosion types during the Mg degradation process, including uniform corrosion [54, 55], localized corrosion [54, 55], flow-induced corrosion [55], erosion corrosion [56], galvanic corrosion [57], stress corrosion [58], atmospheric corrosion, hydrogen cracking [59] and intergranular corrosion [60]. It is worth noting that localized corrosion is always a source of stent fracture. In order to evaluate the biodegradability of Mg implant, a comparison between the anodized and the bare samples under *in vitro* conditions using SBF solution at 37° C up to 30 days usually is carried out. The corrosion rate based on mass loss and Mg^{2+} ions release rate and pH value is shown in **Figure 7a–c**. Both two factors can indicate the biodegradability behavior of Mg and its alloys. The tendency of bare samples to corrosion is significantly different from that of the anodized samples which has more corrosion resistance. The formation of $Mg(OH)_2$ as a corrosion product in bare samples generated once exposed to aqueous solution. Similarly, more Mg ions release from bare samples resulted due to the high degradation and high sensitive surface of Mg. When Mg exposed to a corrosive medium similar to the human plasma corrosion product such as $Mg(OH)_2$ and hydrogen release effect on the pH value of the surrounded solution. In short immersion time, Mg interface exhibits different features especially when treated with the CaP apatite film [61]. For example, when the surface rich with labile ions of CaP it was found to form HA nanoplates, as shown in **Figure 7e**; however, a pours structure formed in the case of apatite film enriched with ZrO_2 NPs, as shown in **Figure 7f**. In contrast, the bare sample exhibits cracks and corrosion occurrence. These results can be attributed to the formation of a porous layer of nanoparticles/plates/rods of the CaP compounds with corrosion products such as magnesium hydroxide and calcium magnesium phosphate.

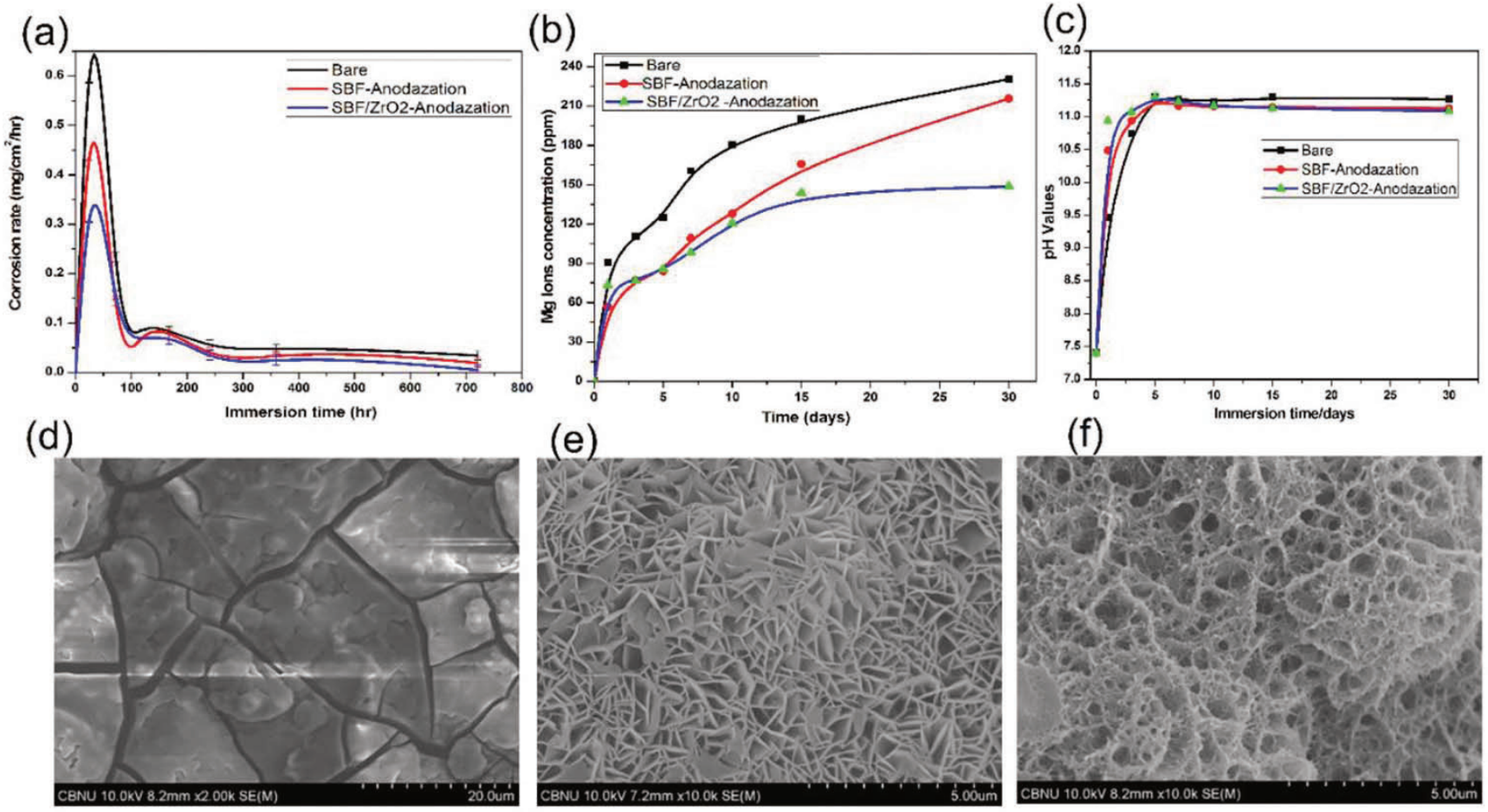

Figure 7. Immersion test results are showing, (a) corrosion rate, (b) Mg ions released and (c) pH value. FESEM images show the surface morphology of (d) bare sample (e) anodized sample in SBF (f) anodized samples in SBF/ZrO_2 NPs after 3 days of immersions in SBF solution at 37°C.

http://dx.doi.org/10.5772/66341

Magnesium sample employed to the anodization technique is more stable in aqueous solutions and corrosive media due to the formation of a thin ceramic layer on the Mg interface. Therefore, Mg biodegradability can be controlled and delayed. An illustrative diagram in **Figure 8b** illustrates a corrosion mechanism before and after anodization treatment in 0.9 NaCl solution. First, the corrosive solution reacts with the substrate interface and starts to corrode and induce cracks and pitting corrosion. Upon increasing the exposure time, anodized film penetrated and the solution reached substrate surface. Thereafter, both the $Mg(OH)_2$ and MgO by means of Cl^- ions penetration are converted and degraded according to the chemical equation:

$$MgO + H_2O \rightarrow Mg^{+2} + 2OH^- \quad (9)$$

Instantaneously, the corrosive solution contact substrate surface Mg^{+2} ions released and hydrogen gas evaluation occurs. As a result, Mg $(OH)_2$ will deposit and react with Cl^- ions to form $MgCl_2$ leading to corrosion occurrence according to the chemical equation:

$$Mg(OH)_2 + Cl^- \rightarrow MgCl_2 \quad (10)$$

The pitting corrosion on the metal surface is due to chloride ions; therefore, the main concept of anodization film is to block Cl^- ions and retard corrosion occurrence on the Mg surface [6].

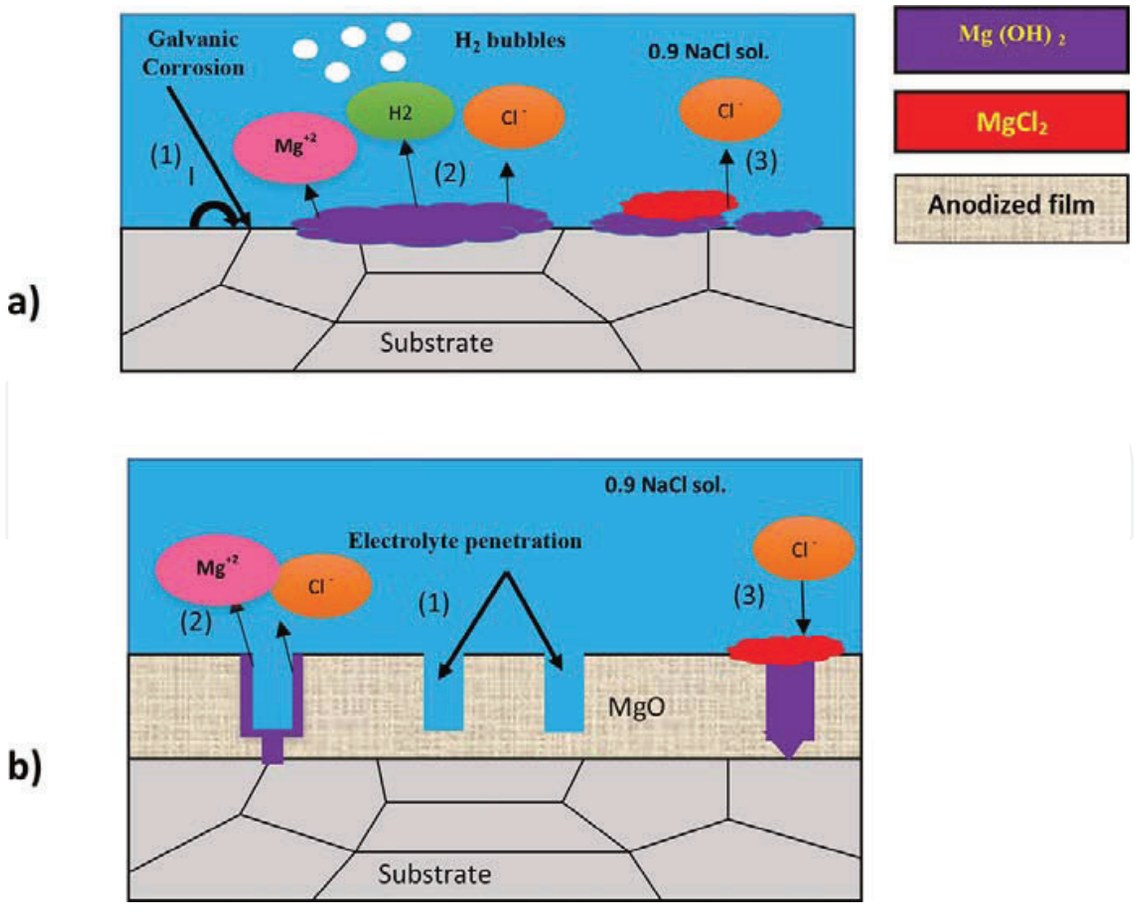

Figure 8. Schematic illustration of the degradation process: (a) bare AZ31 Mg alloy and (b) anodized samples.

6. *In vitro* biocompatibility

Biomaterials must be designed to be biocompatible; however, the majority of biomaterials community has failed to understand the biocompatibility paradigm [62].

Basically, biocompatibility is a characteristic and a complex characteristic at a system and not a material. There are different effects of materials in biological systems as, tissue processing involved in wound healing, the endothelium in contact with intravascular implant devices and the stem cells in bioreactors, the target cells in gene therapy, emphasize that there is no material with complete biocompatibility characteristics [63]. In biodegradable implant such as Mg, bare substrates without any surface modifications show few round shapes of cells on its surface. These attributed to many factors which mainly show corrosion behavior with combined hydrogen gas and induce toxicity to surround tissues. Moreover, surface tribology has additional effect, for example, a rough surface has more cell attachment comparing to smooth one in nanoscale, which behaves as accommodation for cells [64]. In addition, biomimetic nanostructure on the implant surface can enhance biocompatibility and cell proliferation. The Mg substrate that employed to surface modifications using the anodization/hydrothermal process with nanoplate structure shows flat and well-spread features among the nanoplates, as shown in **Figure 9**. Cell proliferation of the extraction of HA nanoplates on the Mg alloy surface finds higher cell proliferation. This can conclude that cells can modify their morphology to match the surface topography as shown in the inset images in **Figure 9**. These findings indicate that how surface modification can influence

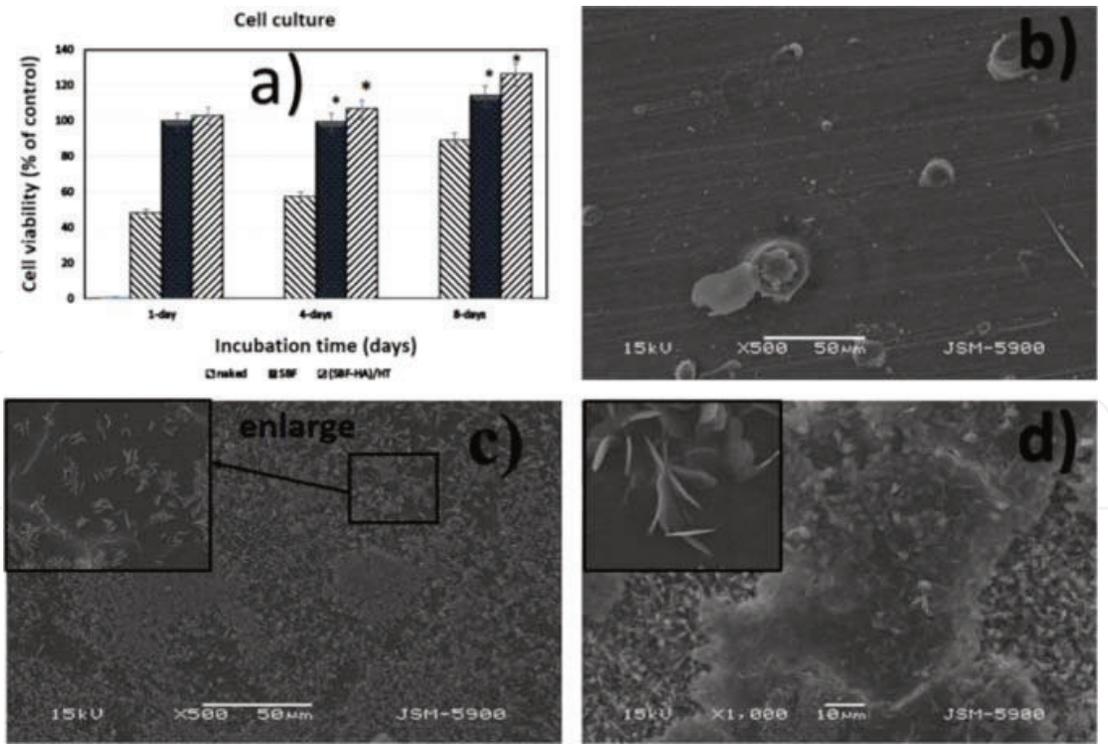

Figure 9. Figure shows the cell viability of anodized/hydrothermal treated Mg samples using cck-8 (a). FESEM images show cell attachment after 5 days (b); naked (c); (SBF-HA) (d); and (SBF-HA)/HT samples. Cell proliferation is presented in means ± STD ($n = 4$) based on ANOVA one-way test (*indicates $p < 0.05$).

http://dx.doi.org/10.5772/66341

surface bioactivity and cell adhesion to the implant interface. Implant surface adheres with the cells and eliminates the mismatch between the surface of the biomaterials and the connected tissue [65]. Extraction of anodized layers shows more cell viability and proliferation as shows in **Figure 10** using confocal microscopic images comparing to the bare substrates extraction.

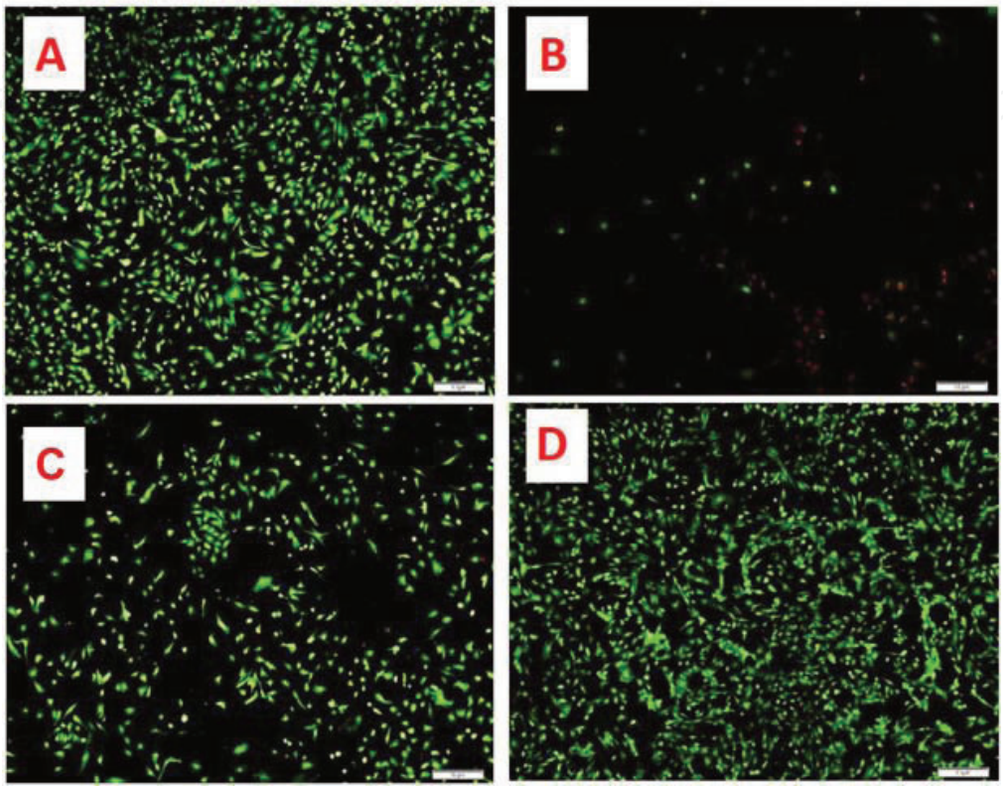

Figure 10. Microscopic florescent images for the live/dead cells of the (a) negative control, (b) positive control, (c) bare sample, (d) AZ31 Mg alloy anodized in SBF at 37°C.

7. Conclusions

Magnesium and its alloys are exhibit biodegradable in physiological media as well as its stiffness close to bone. In addition characteristics of Mg such as low weight, high specific strength and good biocompatibility bring a revolution in medical field toward new generation of biomaterials. However, the high degradation is accompanied by the hydrogen gas effect on the healing of the surrounded tissues. During its healing period, Mg implants lose their mechanical integrity before the bone heals due to the high degradation process. To overcome these limitations, different methods and techniques have been proposed to control the degradation rate of Mg to acceptable levels. Anodization as one of the surface modification techniques finds to increase the surface bioactivity and control degradation rate. In bone substitute Mg acts as a mechanical support during the healing process; moreover, the presence of apatite film on the surface of implant materials can enhance osseointegration of the defected bone. Furthermore, more research studies are devoted to Mg to be used in the future as implant materials in clinical application.

Acknowledgements

This chapter was supported by grant from the Basic Science Research Program through the National Research Foundation of Korea (NRF) by Ministry of Education, Science and Technology (Project no. 2016R1A2A2A07005160) and (Project no NRF-2015R1C1A1A02036404).

Author details

Hamouda M. Mousa[1,2], Chan Hee Park[1]* and Cheol Sang Kim[1]*

*Address all correspondence to: biochan@jbnu.ac.kr and chskim@jbnu.ac.kr

1 Department of Bionanosystem Engineering, Division of Mechanical Design Engineering, Chonbuk National University, Jeonju, Jeonbuk, Republic of Korea

2 Department of Engineering Materials and Mechanical Design, Faculty of Engineering, South Valley University, Qena, Egypt

References

[1] Zhang S, Zhang X, Zhao C, Li J, Song Y, Xie C, et al. Research on an Mg–Zn alloy as a degradable biomaterial. Acta Biomaterialia. 2010;6:626–40.

[2] Heublein B, Rohde R, Kaese V, Niemeyer M, Hartung W, Haverich A. Biocorrosion of magnesium alloys: a new principle in cardiovascular implant technology? Heart. 2003;89:651–6.

[3] Brar HS, Wong J, Manuel MV. Investigation of the mechanical and degradation properties of Mg–Sr and Mg–Zn–Sr alloys for use as potential biodegradable implant materials. Journal of the Mechanical Behavior of Biomedical Materials. 2012;7:87–95.

[4] Zhang E, Xu L, Yu G, Pan F, Yang K. In vivo evaluation of biodegradable magnesium alloy bone implant in the first 6 months implantation. Journal of Biomedical Materials Research Part A. 2009;90A:882–93.

[5] Witte F, Ulrich H, Rudert M, Willbold E. Biodegradable magnesium scaffolds: Part 1: Appropriate inflammatory response. Journal of Biomedical Materials Research Part A. 2007;81A:748–56.

[6] Staiger MP, Pietak AM, Huadmai J, Dias G. Magnesium and its alloys as orthopedic biomaterials: A review. Biomaterials. 2006;27:1728–34.

[7] Kirkland NT, Birbilis N, Walker J, Woodfield T, Dias GJ, Staiger MP. In-vitro dissolution of magnesium–calcium binary alloys: Clarifying the unique role of calcium additions in

bioresorbable magnesium implant alloys. Journal of Biomedical Materials Research Part B: Applied Biomaterials. 2010;95B:91–100.

[8] Witte F, Hort N, Vogt C, Cohen S, Kainer KU, Willumeit R, et al. Degradable biomaterials based on magnesium corrosion. Current Opinion in Solid State and Materials Science. 2008;12:63–72.

[9] Witte F, Kaese V, Haferkamp H, Switzer E, Meyer-Lindenberg A, Wirth CJ, et al. In vivo corrosion of four magnesium alloys and the associated bone response. Biomaterials. 2005;26:3557–63.

[10] Song G, Song S. A possible biodegradable magnesium implant material. Advanced Engineering Materials. 2007;9:298–302.

[11] Chen Y, Xu Z, Smith C, Sankar J. Recent advances on the development of magnesium alloys for biodegradable implants. Acta Biomaterialia. 2014;10:4561–73.

[12] Gray-Munro JE, Seguin C, Strong M. Influence of surface modification on the in vitro corrosion rate of magnesium alloy AZ31. Journal of Biomedical Materials Research Part A. 2009;91A:221–30.

[13] Zhang Y, Yan C, Wang F, Lou H, Cao C. Study on the environmentally friendly anodizing of AZ91D magnesium alloy. Surface and Coatings Technology. 2002;161:36–43.

[14] Guan R-G, Johnson I, Cui T, Zhao T, Zhao Z-Y, Li X, et al. Electrodeposition of hydroxyapatite coating on Mg-4.0Zn-1.0Ca-0.6Zr alloy and in vitro evaluation of degradation, hemolysis and cytotoxicity. Journal of Biomedical Materials Research Part A. 2012;100A:999–1015.

[15] Gao JH, Guan SK, Chen J, Wang LG, Zhu SJ, Hu JH, et al. Fabrication and characterization of rod-like nano-hydroxyapatite on MAO coating supported on Mg–Zn–Ca alloy. Applied Surface Science. 2011;257:2231–7.

[16] Chang WH, Qu B, Liao AD, Zhang SF, Zhang RF, Xiang JH. In vitro biocompatibility and antibacterial behavior of anodic coatings fabricated in an organic phosphate containing solution on Mg–1.0Ca alloys. Surface and Coatings Technology. 2016;289:75–84.

[17] Sabaghi Joni M, Fattah-alhosseini A. Effect of KOH concentration on the electrochemical behavior of coatings formed by pulsed DC micro-arc oxidation (MAO) on AZ31B Mg alloy. Journal of Alloys and Compounds. 2016;661:237–44.

[18] Dou J, Yu H, Chen C, Pan Y, Gao D, Zhang X. Formation of calcium phosphate coating on Mg-Zn-Ca alloy by micro-arc oxidation technique. Materials Letters. 2016;164:575–8.

[19] Sankara Narayanan TSN, Lee MH. Incorporation of ZrO_2 particles in the oxide layer formed on Mg by anodizing: Influence of electrolyte concentration and current modes. Journal of Colloid and Interface Science. 2016;464:36–47.

[20] Gu CD, Yan W, Zhang JL, Tu JP. Corrosion resistance of AZ31B magnesium alloy with a conversion coating produced from a choline chloride—Urea based deep eutectic solvent. Corrosion Science. 2016;106:108–16.

[21] Manoj Kumar R, Kuntal KK, Singh S, Gupta P, Bhushan B, Gopinath P, et al. Electrophoretic deposition of hydroxyapatite coating on Mg–3Zn alloy for orthopaedic application. Surface and Coatings Technology. 2016;287:82–92.

[22] Yu H, Dong Q, Dou J, Pan Y, Chen C. Preparation of Si-containing oxide coating and biomimetic apatite induction on magnesium alloy. Applied Surface Science. part A, 1 December 2016;388:148–154.

[23] Lin B, Zhong M, Zheng C, Cao L, Wang D, Wang L, et al. Preparation and characterization of dopamine-induced biomimetic hydroxyapatite coatings on the AZ31 magnesium alloy. Surface and Coatings Technology. 2015;281:82–8.

[24] Ren Y, Zhou H, Nabiyouni M, Bhaduri SB. Rapid coating of AZ31 magnesium alloy with calcium deficient hydroxyapatite using microwave energy. Materials Science and Engineering: C. 2015;49:364–72.

[25] Chen XB, Nisbet DR, Li RW, Smith PN, Abbott TB, Easton MA, et al. Controlling initial biodegradation of magnesium by a biocompatible strontium phosphate conversion coating. Acta Biomaterialia. 2014;10:1463–74.

[26] Qiu X, Wan P, Tan L, Fan X, Yang K. Preliminary research on a novel bioactive silicon doped calcium phosphate coating on AZ31 magnesium alloy via electrodeposition. Materials Science and Engineering: C. 2014;36:65–76.

[27] Zhang Y, Yan C, Wang F, Li W. Electrochemical behavior of anodized Mg alloy AZ91D in chloride containing aqueous solution. Corrosion Science. 2005;47:2816–31.

[28] Schultze JW, Lohrengel MM. Stability, reactivity and breakdown of passive films. Problems of recent and future research. Electrochimica Acta. 2000;45:2499–513.

[29] Khaselev O, Weiss D, Yahalom J. Structure and composition of anodic films formed on binary Mg–Al alloys in KOH–aluminate solutions under continuous sparking. Corrosion Science. 2001;43:1295–307.

[30] Ismail KM, Virtanen S. Electrochemical behavior of magnesium alloy AZ31 in 0.5 M KOH solution. Electrochemical and Solid-state Letters. 2007;10:C9–C11.

[31] Zhou X, Thompson Ge, Skeldon P, Wood GC, Shimizu K, Habazaki H. Film formation and detachment during anodizing of Al–Mg alloys. Corrosion Science. 1999;41:1599–613.

[32] Barchiche CE, Rocca E, Juers C, Hazan J, Steinmetz J. Corrosion resistance of plasma-anodized AZ91D magnesium alloy by electrochemical methods. Electrochimica Acta. 2007;53:417–25.

[33] Guo XW, Ding WJ, Lu C, Zhai CQ. Influence of ultrasonic power on the structure and composition of anodizing coatings formed on Mg alloys. Surface and Coatings Technology. 2004;183:359–68.

[34] Shi Z, Song G, Atrens A. Corrosion resistance of anodised single-phase Mg alloys. Surface and Coatings Technology. 2006;201:492–503.

[35] Turhan MC, Lynch RP, Jha H, Schmuki P, Virtanen S. Anodic growth of self-ordered magnesium oxy-fluoride nanoporous/tubular layers on Mg alloy (WE43). Electrochemistry Communications. 2010;12:796–9.

[36] Saji VS, Choe HC, Brantley WA. An electrochemical study on self-ordered nanoporous and nanotubular oxide on Ti–35Nb–5Ta–7Zr alloy for biomedical applications. Acta Biomaterialia. 2009;5:2303–10.

[37] Franz S, Rammelt S, Scharnweber D, Simon JC. Immune responses to implants – A review of the implications for the design of immunomodulatory biomaterials. Biomaterials. 2011;32:6692–709.

[38] Nukavarapu SP, Kumbar SG, Brown JL, Krogman NR, Weikel AL, Hindenlang MD, et al. Polyphosphazene/nano-hydroxyapatite composite microsphere scaffolds for bone tissue engineering. Biomacromolecules. 2008;9:1818–25.

[39] Guan J-J, Tian B, Tang S, Ke Q-F, Zhang C-Q, Zhu Z-A, et al. Hydroxyapatite coatings with oriented nanoplate arrays: synthesis, formation mechanism and cytocompatibility. Journal of Materials Chemistry B. 2015;3:1655–66.

[40] Yao Z, Li L, Jiang Z. Adjustment of the ratio of Ca/P in the ceramic coating on Mg alloy by plasma electrolytic oxidation. Applied Surface Science. 2009;255:6724–8.

[41] Srinivasan PB, Liang J, Blawert C, Störmer M, Dietzel W. Characterization of calcium containing plasma electrolytic oxidation coatings on AM50 magnesium alloy. Applied Surface Science. 2010;256:4017–22.

[42] Peixoto Barbosa D, Knörnschild G. Anodization of Mg-alloy AZ91 in NaOH solutions. Surface and Coatings Technology. 2009;203:1629–36.

[43] Wu H-l, Cheng Y-l, Li L-l, Chen Z-h, Wang H-m, Zhang Z. The anodization of ZK60 magnesium alloy in alkaline solution containing silicate and the corrosion properties of the anodized films. Applied Surface Science. 2007;253:9387–94.

[44] Mousa HM, Lee DH, Park CH, Kim CS. A novel simple strategy for in situ deposition of apatite layer on AZ31B magnesium alloy for bone tissue regeneration. Applied Surface Science. 2015;351:55–65.

[45] Mousa HM, Hussein KH, Woo HM, Park CH, Kim CS. One-step anodization deposition of anticorrosive bioceramic compounds on AZ31B magnesium alloy for biomedical application. Ceramics International. 2015;41:10861–70.

[46] Mousa HM, Tiwari AP, Kim J, Adhikari SP, Park CH, Kim CS. A novel in situ deposition of hydroxyapatite nanoplates using anodization/hydrothermal process onto magnesium alloy surface towards third generation biomaterials. Materials Letters. 2016; 164:144–7.

[47] Ye F, Guo H, Zhang H, He X. Polymeric micelle-templated synthesis of hydroxyapatite hollow nanoparticles for a drug delivery system. Acta Biomaterialia. 2010;6:2212–8.

[48] Paital SR, Dahotre NB. Calcium phosphate coatings for bio-implant applications: Materials, performance factors and methodologies. Materials Science and Engineering: R: Reports. 2009;66:1–70.

[49] Dorozhkin SV. Calcium orthophosphate coatings on magnesium and its biodegradable alloys. Acta Biomaterialia. 2014;10:2919–34.

[50] Kim S-M, Jo J-H, Lee S-M, Kang M-H, Kim H-E, Estrin Y, et al. Hydroxyapatite-coated magnesium implants with improved in vitro and in vivo biocorrosion, biocompatibility and bone response. Journal of Biomedical Materials Research Part A. 2014;102:429–41.

[51] Zheng YF, Gu XN, Witte F. Biodegradable metals. Materials Science and Engineering: R: Reports. 2014;77:1–34.

[52] Mousa HM, Hussein KH, Pant HR, Woo HM, Park CH, Kim CS. In vitro degradation behavior and cytocompatibility of a bioceramic anodization films on the biodegradable magnesium alloy. Colloids and Surfaces A: Physicochemical and Engineering Aspects. 2016;488:82–92.

[53] Myrissa A, Agha NA, Lu Y, Martinelli E, Eichler J, Szakács G, et al. In vitro and in vivo comparison of binary Mg alloys and pure Mg. Materials Science and Engineering: C. 2016;61:865–74.

[54] Ghali E, Dietzel W, Kainer K-U. General and localized corrosion of magnesium alloys: A critical review. Journal of Materials Engineering and Performance. 2004; 13:7–23.

[55] Ghali E, Dietzel W, Kainer K-U. Testing of general and localized corrosion of magnesium alloys: A critical review. Journal of Materials Engineering and Performance. 2004;13:517–29.

[56] Ballerini G, Bardi U, Bignucolo R, Ceraolo G. About some corrosion mechanisms of AZ91D magnesium alloy. Corrosion Science. 2005;47:2173–84.

[57] Song G. Recent progress in corrosion and protection of magnesium alloys. Advanced Engineering Materials. 2005;7:563–86.

[58] Yun Y, Dong Z, Lee N, Liu Y, Xue D, Guo X, et al. Revolutionizing biodegradable metals. Materials Today. 2009;12:22–32.

[59] Jones RH. The influence of hydrogen on the stress-corrosion cracking of low-strength Al-Mg alloys. JOM. 2003;55:42–6.

[60] Scamans GM, Holroyd NJH, Tuck CDS. The role of magnesium segregation in the intergranular stress corrosion cracking of aluminium alloys. Corrosion Science. 1987;27:329–47.

[61] Mousa HM, Hussein KH, Raslan AA, Lee J, Woo HM, Park CH, et al. Amorphous apatite thin film formation on a biodegradable Mg alloy for bone regeneration: strategy, characterization, biodegradation and in vitro cell study. RSC Advances. 2016;6:22563–74.

http://dx.doi.org/10.5772/66341

[62] Gallagher WM, Lynch I, Allen LT, Miller I, Penney SC, O'Connor DP, et al. Molecular basis of cell–biomaterial interaction: Insights gained from transcriptomic and proteomic studies. Biomaterials. 2006;27:5871–82.

[63] Williams DF. There is no such thing as a biocompatible material. Biomaterials. 2014; 35:10009–14.

[64] Abdal-hay A, Dewidar M, Lim JK. Biocorrosion behavior and cell viability of adhesive polymer coated magnesium based alloys for medical implants. Applied Surface Science. 2012;261:536–46.

[65] Jones FH. Teeth and bones: applications of surface science to dental materials and related biomaterials. Surface Science Reports. 2001;42:75–205.

IntechOpen